

Fig. S 1: Free-wing impactor during rotation (indicated by the blue arc) depicted with 1.25×10^{-5} s exposure time. Wind is blowing towards the observer. Note the inclined orientation of the sampling substrate on the right relative to the rotation plane, aligned with the sum vector of wind and rotation movement.

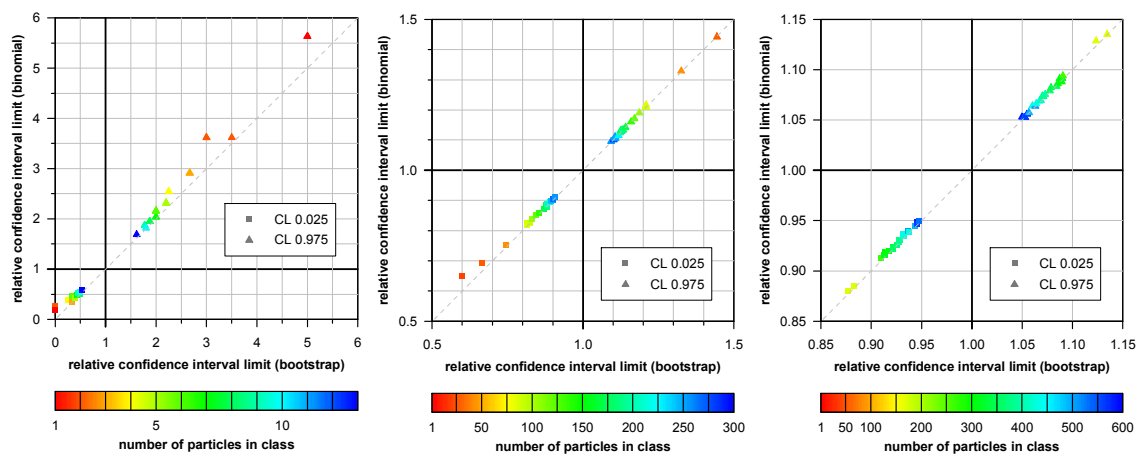


Fig. S 2: Comparison of central 95 % confidence interval limits relative to the relative number abundance of a particle type class. Data basis are the deposition samples at Ragged Point. a: for a low-abundance class (0–1.2 % relative number abundance); b: for a medium-abundance class (2.4–41.8 %); c: for a high-abundance class (27.5–61.9 %). The color shows the absolute number of particles in the according class. Note the different scales between the graphs.

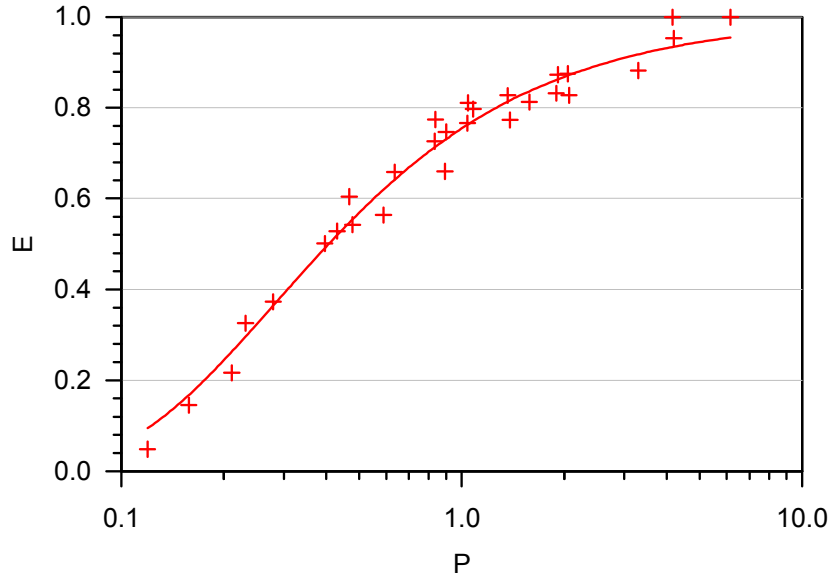


Fig. S 3: Parameterization of collection efficiency E of a disc as function of impact parameter P ; fit to the data of May et al. (1967). Fit function is shown as continuous line.

Table S 1: Conversion formulas used for the calculation of oxide, carbonate, element atomic and ammonium masses, as well as sodium sulfate and sodium chloride volumes. Values were taken from Deer et al. (1992) and Warneck et al. (2012).

$Al_{oxide} = 101.96 \frac{g}{mol} \times \frac{ Al }{2}$ $Si_{oxide} = 60.08 \frac{g}{mol} \times Si $ $P_{oxide} = 141.94 \frac{g}{mol} \times \frac{ P }{2}$ $Ti_{oxide} = 79.88 \frac{g}{mol} \times Ti $ $Fe_{oxide} = 159.69 \frac{g}{mol} \times \frac{ Fe }{2}$	$Na_{oxide} = 61.98 \frac{g}{mol} \times \frac{ Na }{2}$ $Mg_{oxide} = 40.30 \frac{g}{mol} \times Mg $ $K_{oxide} = 94.20 \frac{g}{mol} \times \frac{ K }{2}$ $Ca_{carbonate} = 100.09 \frac{g}{mol} \times Ca $
$Na_{mass} = 22.99 \frac{g}{mol} \times Na $ $Mg_{mass} = 24.31 \frac{g}{mol} \times Mg $ $K_{mass} = 39.10 \frac{g}{mol} \times K $ $Ca_{mass} = 40.08 \frac{g}{mol} \times Ca $	$Cl_{mass} = 35.45 \frac{g}{mol} \times Cl $ $SO_{4,mass} = 96.06 \frac{g}{mol} \times S $ $NH_{4,mass} = -18.04 \frac{g}{mol} \times c_{dust}$ $NO_{3,mass} = 62.00 \frac{g}{mol} \times c_{dust}$
$Na_2SO_{4,volume} = \frac{142.04 \frac{g}{mol} \times X }{2.66 \frac{g}{cm^3}} \begin{cases} X = Na, \text{ if classified as insoluble sulfate} \\ X = S \text{ in other cases} \end{cases}$ $NaCl_{volume} = \frac{58.44 \frac{g}{mol} \times Cl }{2.17 \frac{g}{cm^3}}$	

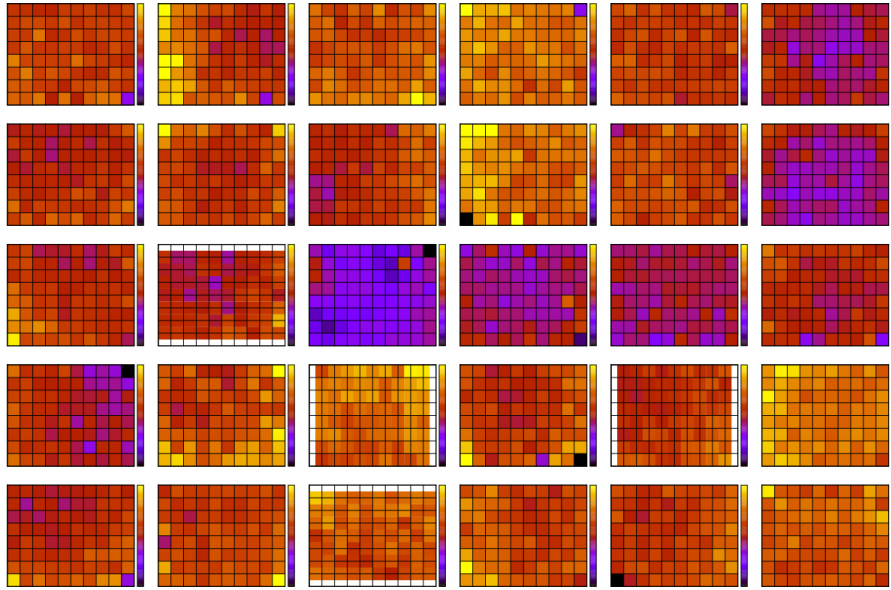


Fig. S 4: Maps of particle deposition density on the FWI substrates for $4\ \mu\text{m} < d_g < 8\ \mu\text{m}$. Each division on the x and y axes equals 1 mm distance. Color bar range is 0 to 1000 particles per mm^2 . Lower panel: $4\ \mu\text{m} < d_g < 8\ \mu\text{m}$, color bar range is 0 to 2500 particles per mm^2

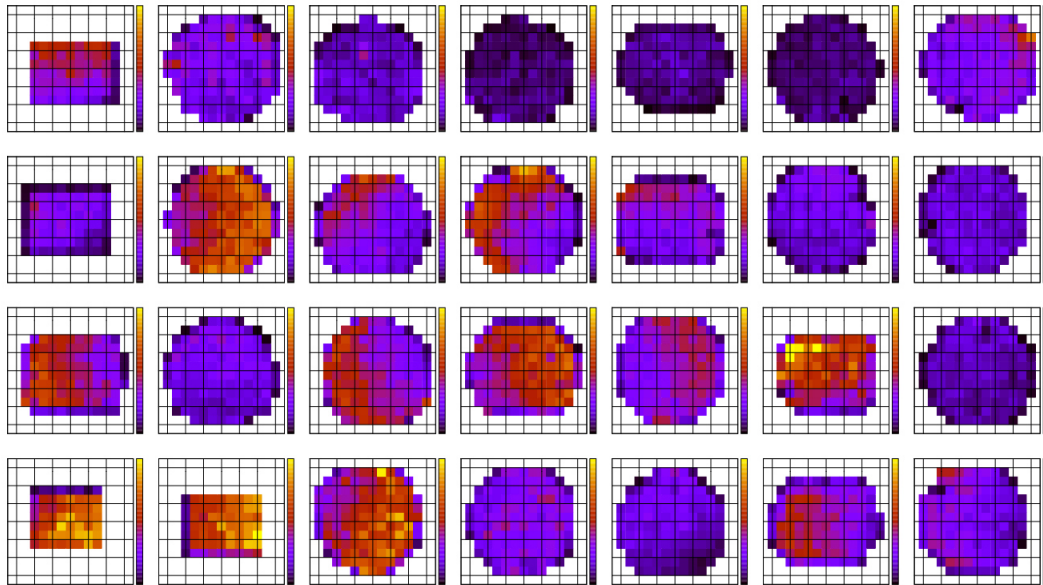


Fig. S 5: Maps of particle deposition density on the DPDS substrates for $4\ \mu\text{m} < d_g < 8\ \mu\text{m}$. Each division on the x and y axes equals 2 mm distance. Color bar range is 0 to 600 particles per mm^2 .

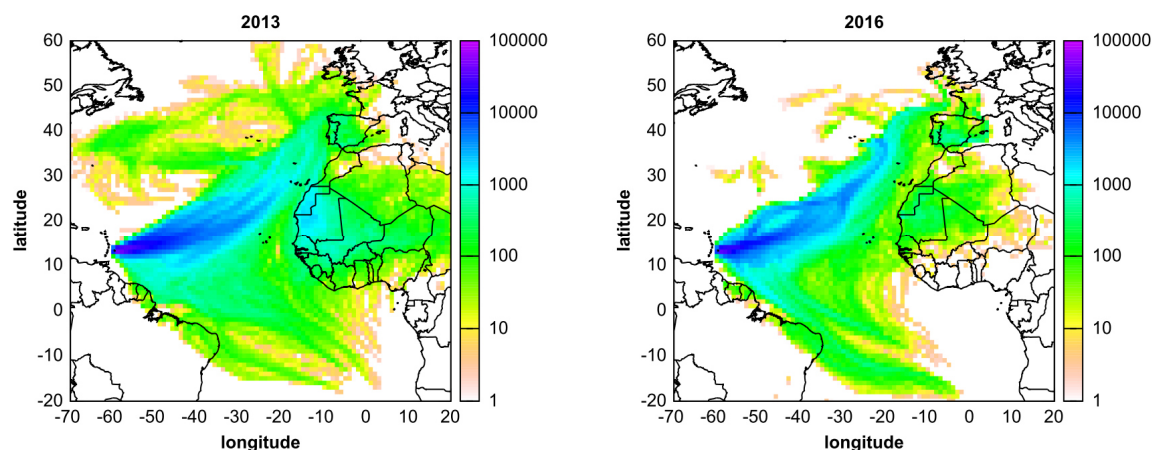


Fig. S 6: Potential air mass provenance during the measurement campaigns 2013 and 2016. A location is counted as potential provenance, if the trajectory at this point is lower than modeled boundary layer height. Colors indicate number of according trajectory point for each grid cell, corrected for differences in grid cell area.

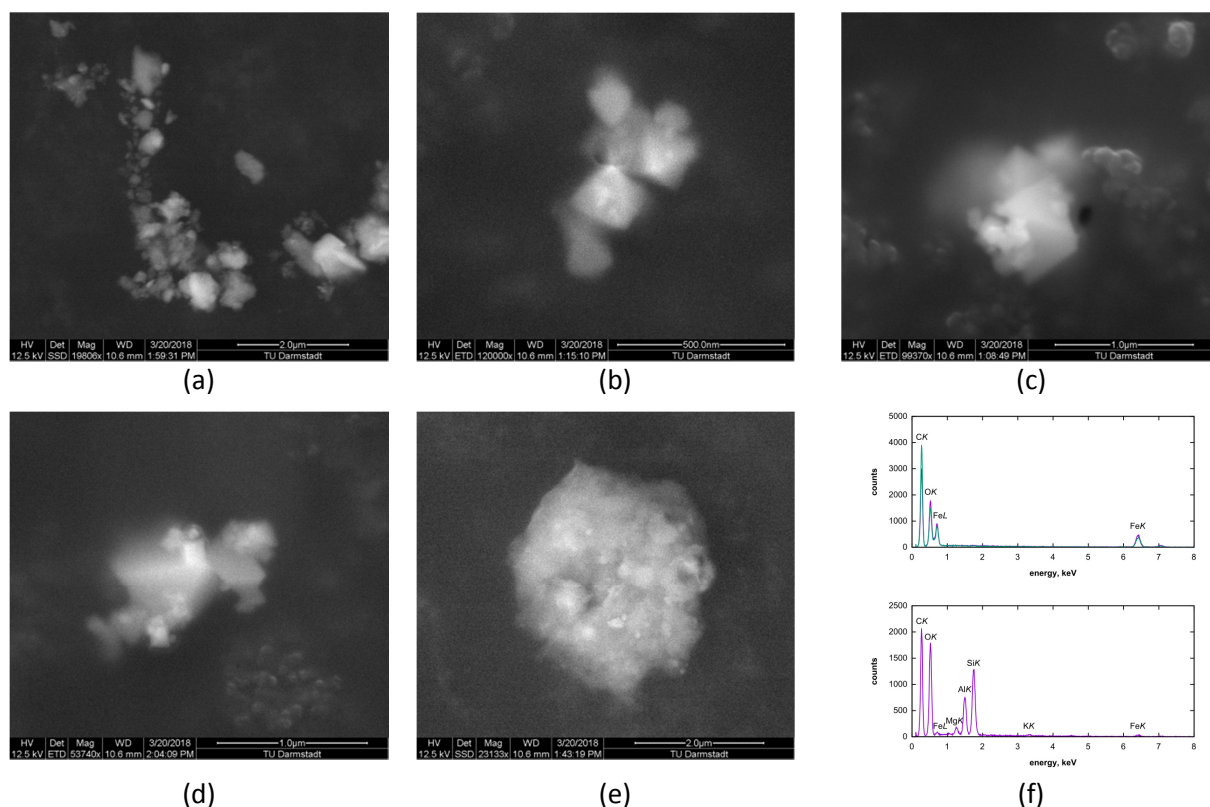


Fig. S 7: Electron images of small Fe-rich particles (a-d) and a Fe-containing silicate (e) deposited at Ragged Point in 2016 during air mass advection from South America. The upper part of f shows typical examples of X-ray spectra of the Fe-rich particles, the lower the spectrum of the silicate (e). Characteristic X-ray peaks are labeled, C and in part O are contained in the substrate.

Table S 2: 95 % quantile of the fractions of internally mixed particles due to coincidental mixture on the substrate, for a two-component system with CV-ground size distribution. Strong mixture refers to a minimum particle volume fraction of the other component of 20 %, detectable mixture refers to 1 %. Only values larger than 0.001 are shown, values larger than 0.05 are highlighted in bold.

<u>strong mixture</u>		size range, μm						
component ratio	apparent area coverage	>1-2	>2-4	>4-8	>8-16	>16-32	>32-64	>64-128
50 % / 50 %	0.001				.007			
	0.005			.002	.007	.027		
	0.010			.002	.010	.032	.042	
	0.025		.001	.003	.018	.051	.038	
	0.048		.001	.004	.032	.084	.044	.077
	0.071		.001	.006	.045	.116	.053	.077
	0.093		.002	.007	.057	.145	.064	.086
	0.172	.001	.002	.012	.102	.254	.121	.108
90 % / 10 %	0.001							
	0.005			.002	.003	.014		
	0.010				.004	.018		
	0.025		.001	.001	.007	.023	.024	
	0.048			.002	.012	.034	.023	.059
	0.071			.002	.017	.045	.025	.050
	0.093			.003	.021	.055	.031	.040
	0.172		.001	.005	.037	.091	.046	.051
99 % / 1 %	0.001							
	0.005				.001			
	0.010					.006		
	0.025				.001	.005		
	0.048				.002	.006	.010	
	0.071				.002	.007	.008	
	0.093				.003	.008	.006	
	0.172				.005	.011	.008	.016
<u>detectable mixture</u>		size range, μm						
component ratio	apparent area coverage	>1-2	>2-4	>4-8	>8-16	>16-32	>32-64	>64-128
50 % / 50 %	0.001				.008	.043		
	0.005			.003	.011	.050	.167	
	0.010		.003	.003	.015	.071	.158	.250
	0.025		.002	.005	.029	.125	.214	.286
	0.048		.003	.008	.054	.206	.327	.333
	0.071	.001	.003	.011	.077	.284	.427	.409
	0.093	.001	.004	.014	.098	.354	.526	.500
	0.172	.002	.007	.025	.176	.563	.777	.836
90 % / 10 %	0.001							
	0.005			.002	.005	.027	.100	
	0.010			.002	.007	.034	.083	
	0.025		.001	.002	.012	.051	.104	.167
	0.048		.001	.003	.020	.083	.146	.182
	0.071		.002	.004	.029	.110	.178	.200
	0.093		.002	.005	.037	.133	.210	.217
	0.172		.003	.010	.065	.221	.331	.294
99 % / 1 %	0.001							
	0.005				.002			
	0.010				.002	.007		
	0.025				.002	.010	.026	
	0.048				.003	.013	.029	.067
	0.071				.004	.015	.033	.056
	0.093				.005	.018	.035	.049
	0.172			.001	.008	.027	.050	.053

Table S 3: 95 % quantile of the fractions of internally mixed particles due to coincidental mixture on the substrate, for a two-component system with CV-air size distribution. Strong mixture refers to a minimum particle volume fraction of the other component of 20 %, detectable mixture refers to 1 %. Only values larger than 0.001 are shown, values larger than 0.05 are highlighted in bold.

<u><i>strong mixture</i></u>		size range, μm						
component ratio	apparent area coverage	>1-2	>2-4	>4-8	>8-16	>16-32	>32-64	>64-128
50 % / 50 %	0.001			.005				
	0.005		.001	.004	.007	.014		
	0.010		.002	.005	.009	.020	.053	
	0.025		.003	.010	.016	.032	.049	
	0.048		.005	.017	.027	.052	.059	
	0.093	.002	.010	.032	.049	.090	.090	.154
	0.134	.002	.014	.046	.070	.128	.127	.167
	0.173	.003	.019	.060	.092	.166	.163	.176
90 % / 10 %	0.001							
	0.005			.002	.003	.012		
	0.010			.002	.004	.011		
	0.025		.001	.004	.007	.014	.024	
	0.048		.002	.007	.011	.021	.031	
	0.093		.004	.012	.019	.034	.039	.111
	0.134		.005	.017	.027	.049	.053	.091
	0.173	.001	.007	.022	.034	.061	.063	.095
99 % / 1 %	0.001							
	0.005							
	0.010				.001			
	0.025				.002	.002		
	0.048			.001	.002	.004	.010	
	0.093			.002	.003	.005	.009	
	0.134			.002	.003	.007	.012	
	0.173			.003	.004	.008	.011	.053
<u><i>detectable mixture</i></u>		size range, μm						
component ratio	apparent area coverage	>1-2	>2-4	>4-8	>8-16	>16-32	>32-64	>64-128
50 % / 50 %	0.001		.002	.005	.013	.050		
	0.005		.002	.008	.020	.043	.125	
	0.010		.003	.012	.029	.059	.143	
	0.025	.001	.006	.024	.059	.106	.186	.500
	0.048	.002	.010	.045	.108	.188	.278	.521
	0.093	.003	.019	.085	.199	.329	.453	.667
	0.134	.004	.028	.121	.278	.453	.599	.750
	0.173	.006	.037	.156	.352	.556	.714	.864
90 % / 10 %	0.001			.005	.011			
	0.005		.001	.004	.009	.022	.071	
	0.010		.001	.005	.013	.027	.071	
	0.025		.002	.010	.024	.045	.093	.333
	0.048		.004	.017	.041	.073	.124	.333
	0.093	.001	.007	.031	.073	.126	.185	.333
	0.134	.002	.010	.045	.104	.171	.236	.400
	0.173	.002	.014	.057	.131	.213	.287	.409
99 % / 1 %	0.001							
	0.005			.001	.003	.011		
	0.010			.001	.003	.006		
	0.025			.002	.004	.009	.023	
	0.048			.002	.006	.012	.027	
	0.093			.004	.009	.017	.029	.111
	0.134		.001	.005	.013	.022	.036	.111
	0.173		.002	.007	.016	.027	.044	.111

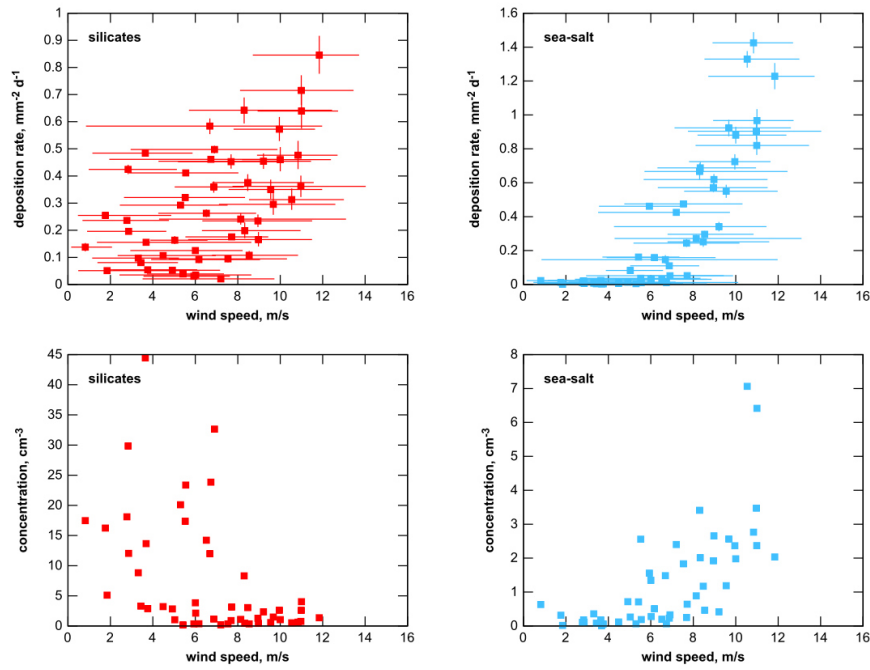


Fig. S 8: Total number deposition rate (upper graphs) and total number concentrations calculated with the Piskunov model (lower graphs) for all samples of 2013 and 2016 as function of wind speed for silicate and sea-salt particles. In the upper graphs, variation in wind speed is given as central 95 % quantile of 1-minute averages, and statistical uncertainty of the deposition rate is shown as two-sided 95 % confidence interval.

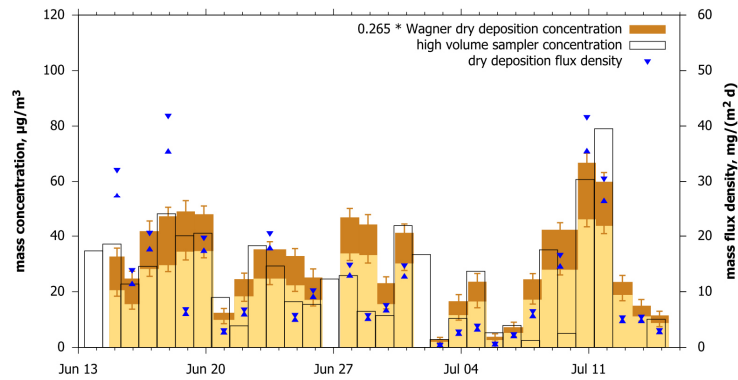


Fig. S 9: Dust mass concentration and flux density time series derived from DPDS data with a linearly tuned Wagner deposition velocity model, compared to such obtained from the a high-volume sampler (Kristensen et al. 2016). The darker brown bar shows the range from lower to upper estimate, the blue triangles the lower and upper estimate of dust deposition flux density.

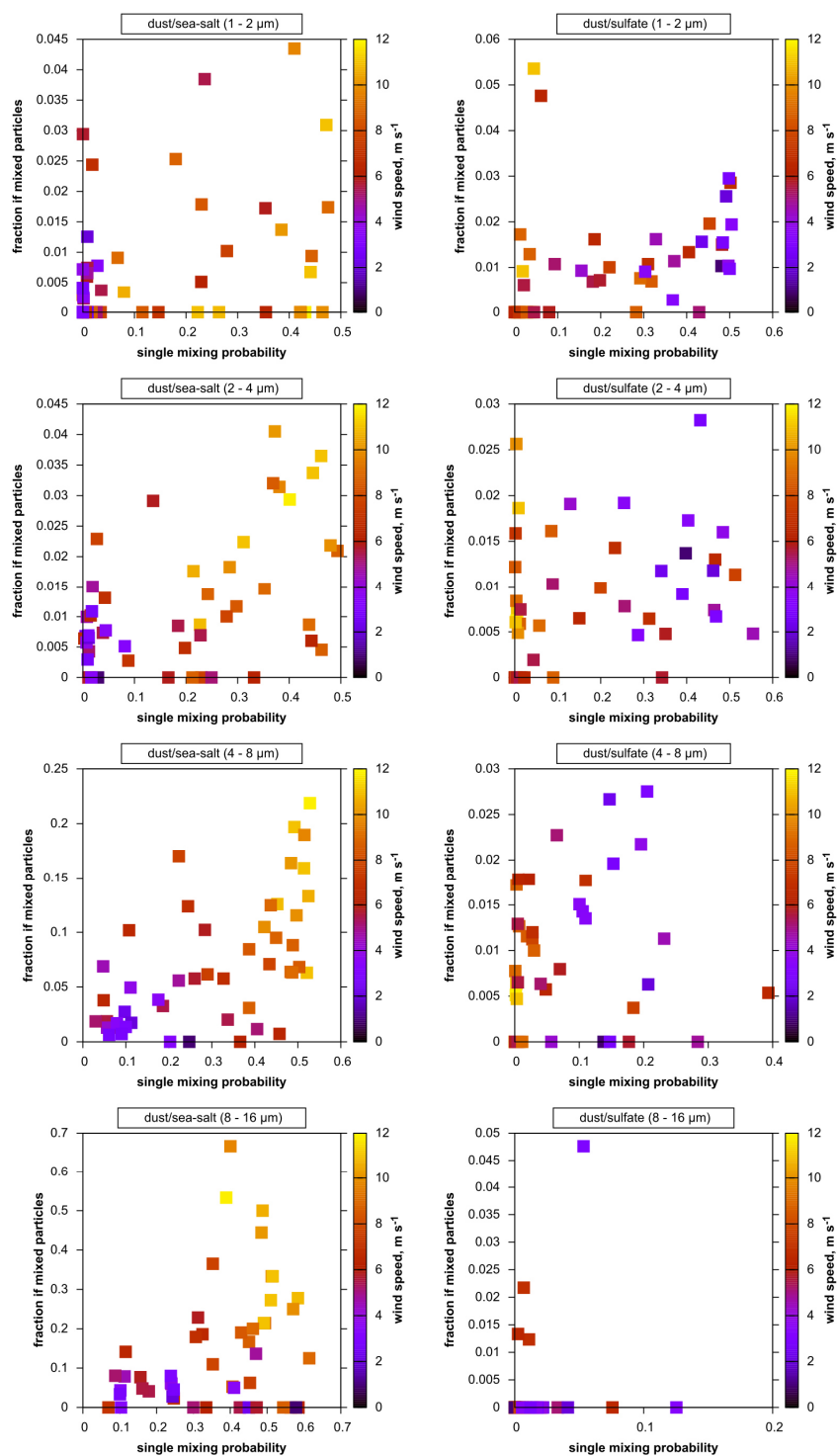


Fig. S 10: Ratio of binary mixed particle abundance to according pure compound abundance as function of the size-restricted single mixing probability. Deposition rate is color coded.